



Published in final edited form as:

J Mater Chem B. 2019 October 07; 7(37): 5688–5694. doi:10.1039/c9tb01597c.

Polyphenol-based nanoplatform for MRI/PET dual-modality imaging guided effective combination chemotherapy

Jingjing Wang^{a,d,f}, Wei Sang^{b,c,f}, Zhen Yang^d, Zheyu Shen^d, Zhantong Wang^d, Orit Jacobson^d, Yundai Chen^a, Yong Wang^e, Mingyan Shao^e, Gang Niu^d, Yunlu Dai^{b,c,*}, Xiaoyuan Chen^{d,*}

^a.Department of Cardiology, Chinese PLA General Hospital, Beijing 100853, China.

^b.Cancer Centre, Faculty of Health Sciences, University of Macau, Macau SAR 999078, China.

^c.Institute of Translational Medicine, Faculty of Health Sciences, University of Macau, Macau SAR 999078, China.

^d.Laboratory of Molecular Imaging and Nanomedicine (LOMIN), National Institute of Biomedical Imaging and Bioengineering (NIBIB), National Institutes of Health (NIH), Bethesda, MD 20892, USA.

^e.School of Life Science, Beijing University of Chinese Medicine, Beijing 100029, China.

^f.Authors have equally contributed to the work.

Abstract

Combination therapy with multiple chemotherapeutic agents is the main approach for cancer treatment in clinic. Polyphenol-based materials are found in our diet, demonstrate good biocompatibility, and prevent numerous diseases. In this study, we encapsulate two drugs in a single polyphenol-based polymer with Fe³⁺ or Mn²⁺ ions as the cross-linkers for cancer therapy. The combination index of the two drugs is an essential parameter to evaluate the drug combinations. The amphiphilic polymer, poly(ethylene glycol)-block-polydopamine (PEG-PDA), was prepared by RAFT polymerization. The nanoparticles were prepared via self-assembly with Fe³⁺ or Mn²⁺ ions. Both doxorubicin (DOX) and simvastatin (SV) were encapsulated in the core of nanoparticles. The cell viability and combination index were evaluated in vitro. The tumor accumulation of nanoparticles was investigated by positron-emission tomography (PET) and magnetic resonance (MR) imaging. The as-prepared nanoparticles exhibited high drugs loading capacity. The drug loaded nanoparticles could kill the cancer cells effectively with a combination index < 1. Both PET and MRI revealed that the nanoparticles showed long blood circulation time and high tumor accumulation. The nanoparticles could inhibit tumor inhibition via intravenous

* yldai@um.edu.mo, shawn.chen@nih.gov.

Conflicts of interest

The authors have declared that no competing interest exists.

Additional information

Supplementary data to this article can be found online.

Electronic Supplementary Information (ESI) available: [details of any supplementary information available should be included here].
See DOI: [10.1039/x0xx00000x](https://doi.org/10.1039/x0xx00000x)

injection of nanoparticles. The polyphenol-based nanoplatform may serve as a promising theranostic candidate for clinical application

Introduction

Nanomedicine in combination with cancer diagnosis and therapy, has recently gained extensive attention in cancer imaging and treatment.^{1, 2} Smart polymers with stimuli-responsive property are promising as diagnostic drug carriers for imaging-guided cancer therapy.^{3–5} Bioinspired catechol-functionalized polymers have high structural stability by metal crosslinker to hold loaded drugs within the cores in blood circulation, and the polymers can trigger drug release in the tumor site.^{6–8} Notably, various metals can be employed as crosslinkers to coordinate catechols to achieve a range of properties^{9–12}. For instance, adjacent hydroxyl groups provide chelating sites for Fe³⁺ thereby resulting in metal-phenolic networks easily. Furthermore, Fe³⁺ is readily available and inexpensive.¹⁰ Mn²⁺ can be employed as magnetic resonance imaging (MRI) contrast agents,⁹ and the isotope Copper-64 (⁶⁴Cu) and Zirconium-89 (⁸⁹Zr) are good candidates for positron-emission tomography (PET) imaging.^{13, 14} Therefore, catechol-functionalized polymers are the interesting candidates for nanomedicine applications.

Cancer has become one of the most devastating diseases worldwide.¹⁵ Chemotherapy remains the preferred treatment for cancer in clinical settings. Integrating drug delivery and in situ diagnostics into one platform is a promising strategy for clinical applications.^{16, 17} Moreover, how to reduce the side effects of anticancer drugs on normal organs is still a challenge. Doxorubicin (DOX) is a classic anti-cancer drug in clinical settings with inhibition of topoisomerase II activity in cells.¹⁸ However, the highly toxic DOX could lead to undesirable cardiotoxicity.¹⁹ Simvastatin (SV) is one of the most essential drugs to reduce the synthesis of downstream non-sterol products²⁰. SV still exhibits anti-cancer activity by targeting cell cycle arrest and the depletion of cholesterol precursors.^{21, 22} The independent mechanism can accomplish synergistic therapy.^{23–25} Additionally, SV can protect the heart and reduce cardiotoxicity.²⁰ Therefore, the SV/DOX combination therapy is one of the promising approaches in clinical settings.^{24, 26}

Here, we report a promising metal-phenolic networks (MPNs) based nanoplatform by integrating synergistic cancer treatment and bioimaging. A block polymer poly(ethylene glycol)-block-polydopamine (PEG-PDA) was synthesized by reversible addition-fragmentation chain transfer (RAFT) polymerization. Both DOX and SV were encapsulated in the core of the polymer with Fe³⁺ metal as cross-linkers to prepare PEG-PDA-Fe@DOX/SV nanoparticles (PFDS NPs, Scheme 1). DOX and SV-encapsulated PFDS NPs exhibited promising synergistic effects and accumulated in the tumor by the EPR effect. Moreover, Mn²⁺ could be employed as a crosslinker in place of Fe³⁺ as the MRI contract agents. Zirconium-89 (⁸⁹Zr) with a relatively long half-life was employed to chelate with polyphenols for PET imaging. The PFDS NPs could accumulate in the tumor and improve therapeutic efficacy compared with free drugs. This promising strategy demonstrates a new avenue for SV-based synergistic cancer theranostics.

Experimental section

Polymer preparation.

The polymer precursor PEG₅₀₀₀-poly(pentafluorophenyl methacrylate) (-PPFMA) was synthesized according to the reported method.²⁷ In brief, poly(ethylene glycol) methyl ether 2-(dodecylthiocarbonothioylthio)-2-methylpropionate (PEG DDMAT macroCTA, 100 mg, 0.02 mmol), azobisisobutyronitrile (AIBN, 0.164 mg, 0.001 mmol) and pentafluorophenyl methacrylate (PFMA, 151.2 mg, 0.6 mmol) were dissolved in 1,4-dioxane (2 mL) under magnetic stirring. The reaction mixture was bubbled with nitrogen for 1 h, and the above solution was heated at 70 °C in an oil bath for 24 h. The above solution was kept on ice for 1 h, diluted with tetrahydrofuran (THF, 10 mL), and precipitated into diethyl ether (200 mL). The above processes were repeated for four times to remove monomer entirely. The resulting solid polymer was dried by an evaporator. The removal of thioester is essential to inhibit the polymers crosslinking process, which may happen during post-functionalization of PEG₅₀₀₀-PPFMA. The thioester of PEG₅₀₀₀-PPFMA was removed with 100 equivalent AIBN. Finally, the precursor polymer PEG₅₀₀₀-PPFMA was obtained by precipitating in diethyl ether.

For the synthesis of PEG₅₀₀₀-PDA₂₅ copolymer, PEG₅₀₀₀-PPFMA (0.1 g) and dopamine hydrochloride (0.2 g, 1.1 mmol) were added in THF (10 mL). Triethylamine with the same molar weight of dopamine hydrochloride (0.20 g, 1.1 mmol) was added into the mixture and stirred at 60 °C under nitrogen protection overnight. The reaction mixture was dialyzed against H₂O for 3 days. Finally, PEG₅₀₀₀-PDMA₂₅ (0.9 g) was obtained after lyophilization. The number of DMA in one polymer was calculated for ~25 by the ¹H NMR spectrum (Fig. S1). In addition, the whole synthesized procedure of the PEG₅₀₀₀-PDA₂₅ copolymer is provided in Fig. S2.

The therapeutic PFDS NPs preparation.

The hydrophobic DOX was prepared by mixing DOX HCl (3 mg) with TEA (7.7 μL) in DMF (1 mL) and stirred overnight. PDA-PEG (2 mg/mL) was dissolved in DMF (1 mL) together with SV (2 mg/mL, 0.5 mL) and DOX (0.2 mL). Subsequently, FeCl₃ (3 mg/mL in H₂O, 0.1 mL) and H₂O (2 mL) were added to the above DMF mixture and stirred for 1 h. PBS buffer (3 mL) was added into the mixture and stirred overnight. DMF was removed from the system by dialysis (~3500 MWCO) for 24 h.

Cytotoxicity of NPs, DOX, SV and DOX & SV combination in vitro

U87MG cells were used to investigate the cytotoxicity of PFDS NPs by MTT assay. U87MG cells were seeded in 96-well plates with a density of 5000 per well in MEM supplemented with 10% FBS and then incubated overnight. PFDS NPs, DOX, SV and DOX & SV combination at different concentrations were added into each well and incubated for 48 h. MTT solution (5 mg/mL, 10 μL) was added into each well for another 4 h. The medium was removed and DMSO was added to dissolve formazan crystal in each well. Finally, the absorbance of formazan solution was measured at 570 nm.

Cell uptake experiment

The PFDS NPs were labelled with Alexa Fluor 488 dye (AF488) by conjugating the AF488 cadaverine with PEG-PDA by Michael adduct formation²⁸. The cell uptake experiment was investigated by incubating AF488-NPs with U87MG cell under various time. The percentage of cells associated with PFDS NPs was assessed by flow cytometry. In a typical experiment, the U87MG cells were incubated with AF488- PFDS NPs for 1, 4, 12 and 24 h. At different timepoints, the U87MG cells were washed by PBS three times and subjected to flow cytometry.

Multicellular tumor spheroids (MCS)

First, the Ce6-labelled PFDS NPs were designed and prepared by encapsulating Ce6 in the core of the NPs. MCS was prepared by a previously reported procedure¹³. Corning® Spheroid Microplates (96-well plates) were employed as the plates for MCS construction. U87MG cells were seeded in 96-well plates with 1000 cells per well and spun down with 3,000 rcf for 5 min. The cells were cultured in the wells for 5 days to gain the MCS. The Ce6 labelled PFDS NPs were incubated with MCS for 24 h and the MCS was washed by PBS and fixed by Z-fix solution. The nucleus was stained by DAPI. Finally, the MCS was observed by a Zeiss LSM 780 confocal microscopy.

Results

Self-assembly and characterization of nanoparticles

First, the polymer precursor poly(ethylene glycol)-block-poly(pentafluorophenyl methacrylate) (PEG₅₀₀₀-PPFMA₂₅) was synthesized by RAFT polymerization. PFMA was replaced by dopamine to gain poly(ethylene glycol)-block-polydopamine (PEG-PDA). The NMR spectra in Fig. S1 confirmed the structure of PEG-PDA. For nanoparticles preparation, both DOX and SV were dissolved in DMF and encapsulated in PEG-PDA in the presence of Fe³⁺ by adjusting the pH to 7.8 with Tris buffer. The above solution was dialyzed against H₂O for 24 h to gain PEG-PDA-Fe@DOX/SV nanoparticles (PFDS NPs). As given in Fig. 1a, the size of nanoparticles was around 75 nm, which was consistent with the dynamic light scattering (DLS) result (Fig. 1c). The drug loading efficiencies of DOX and SV were 10.2 % and 16.0 %, respectively. Mn²⁺ was used as the crosslinker instead of Fe³⁺ by the same procedure to gain PEG-PDA-Mn@DOX/SV nanoparticles. TEM image indicated that monodispersed Mn-based PFDS NPs were obtained with the size around 65 nm, which matched well with the DLS result (Fig. 1d).

Cell uptake, cell viability, and nanoparticles penetration evaluation by multicellular spheroid model

Furthermore, the cell association was determined by incubation of PFDS NPs with cells for various times. The confocal microscopy images were displayed in Fig. 2a, the PFDS NPs were found in the cytoplasm after 2 h of incubation by endocytosis. Then red fluorescence was observed in both the cytoplasm and nucleus after incubation with PFDS NPs for 8 h. When the incubation time increased to 24 h, strong fluorescence and incomplete cell membrane were observed in the nucleus, indicating the cell death by DOX released from

PFDS NPs. Cell uptake was also evaluated by flow cytometry by incubating AF488 labelled PFDS NPs with cells (Fig. S3). Comparison with the control group, the fluorescence of cells increased as the incubation time was prolonged.

To investigate the cytotoxicity of PFDS NPs, the cell viability of U87MG was further investigated by 3-(4,5-dimethylthiazol-2-yl)-2,5-diphenyltetrazolium bromide (MTT) assay. The free DOX, free SV and free DOX+SV combination were employed as control groups. As shown in Fig. 2b–c, all the groups exhibited concentration-dependent toxicity to U87MG cells. The half maximal inhibitory concentration (IC_{50}) of free DOX, free SV, free DOX+SV and PFDS NPs were 0.76, 7.15, 0.39 and 0.31 μM (Table S1), respectively. Furthermore, the combination index (CI) was calculated according to previously reported procedure¹³. The CI of free drugs combination and PFDS NPs were 0.32 and 0.49 (Table S2), respectively. The above CI values were both lower than 1, which indicated strong synergistic effects against U87MG cells. The above results suggested that the PFDS NPs could promote the therapeutic efficacy of drugs.

The solid tumor tissue is a dense structure with an extracellular matrix, which may hinder nanomaterials diffusion. Therefore, nanoparticles penetration ability to solid tumor is a big challenge for delivery of drugs into tumor cells. We investigated the penetration of PFDS NPs by a 3D multicellular spheroid (MCS) model based on U87MG cells, which could provide a dense barrier for nanoparticles penetration. Chlorin e6 (Ce6) was encapsulated in the PFDS NPs with drugs together. Ce6-PFDS NPs were co-cultured with MCS for 1 day, and representative confocal microscopy images from various layers (top, middle, and bottom) were given in Fig. 3. The red fluorescence can be observed not only on the edge of the MCS, but also in the middle of it. The above results indicated that the PFDS NPs could penetrate into the spheroids, which is suitable for further clinic application.

In vivo MR and PET imaging and cancer combination chemotherapy

MRI is an essential medical imaging technique for cancer diagnosis with high spatial resolution²⁹. Mn-based MRI contrast agents (CAs) have exhibited excellent MRI ability due to their paramagnetic property and good biocompatibility^{30–32}. Herein, we made use of Mn^{2+} based PFDS NPs as contrast agents for MRI by exploiting the coordination between Mn^{2+} and polyphenols. As given in Fig. 4a, the T_1 MRI signals increased by Mn concentration with r_1 value of $7.3 \text{ mM}^{-1} \text{ S}^{-1}$. Furthermore, the whole body T_1 -weighted MR images of U87MG tumor mice were further investigated (Fig. 4b–f). The Mn-PFDS NPs were injected to the mouse by tail vein, and a significant T_1 contrast improvement was observed clearly in the tumor site at 48 h post injection. The above results indicated that the Mn-PFDS NPs could be employed as contrast agent for MR imaging and accumulate in the tumor for further therapeutic application.

Positron emission tomography (PET) imaging is an essential approach to investigate nanomaterials biodistribution and tumor accumulation. Herein, Zirconium-89 (^{89}Zr) with the relatively long half-life ($t_{1/2} = 78.4 \text{ h}$) were used to chelate with polyphenols in PFDS NPs for PET imaging. Representative whole-body PET images of U87MG cell xenograft mice at various post-injection time points were provided in Fig. 5a. The tumor accumulation could increase from 4.1 % of injected dose per gram of tissue (% ID/g) to 6.1 % ID/g when the

post-injection time was prolonged from 1 h to 48 h (Fig. 5b). There was still 5.1 % ID/g in the tumor site after 72 h (Fig. S6). Interestingly, only 14.1 % ID/g of PFDS NPs was located in the liver at 72 h post-injection, which could reduce side effect of PFDS NPs on the normal organs. In addition, less than 2.2 % ID/g of PFDS NPs was detected in the bone owing to the stable chelation between ^{89}Zr and polyphenols.

The antitumor activity of PFDS NPs was further evaluated with the U87MG xenograft tumor model. All the xenograft tumor mice were randomly divided into five groups: PBS, free DOX (1 mg/kg), free SV (1.6 mg/kg), free DOX + free SV (DOX: 1 mg/kg; SV: 1.6 mg/kg) and PFDS NPs (DOX: 1 mg/kg; SV: 1.6 mg/kg). All the mice were treated with different formulas on day 1st, 3rd and 5th for three times. As shown in Fig. 6a, treatment with single drug or free drugs combination showed negligible tumor inhibition. The PFDS NPs treated group exhibited the best tumor inhibition behavior, the tumor volumes were much smaller than the free drugs combination (Fig. 6b, $P < 0.01$). Additionally, there is no obvious mice body weight reduction (Fig. 6c). The tumor slices by haematoxylin and eosin (H&E) staining after 7 days of treatment were given in Fig. 6d. The tumor cell were severely damaged from the PFDS NPs treated group. These results indicated the PFDS NPs were located in the tumor and improve the chemotherapy effect. H&E staining results of normal organs were provided in Fig. S7, No noticeable damage, necrosis, or inflammation were not reported, indicating the good biocompatibility and no obvious side effect of PFDS NPs to normal organs.

Conclusions

In conclusion, we developed polyphenol-based DOX and SV co-loaded PFDS NPs for MRI/PET dual-modality imaging guided combination therapy. Both DOX and SV could be encapsulated in the core of PFDS NPs and they exhibit synergistic combination effect. The Mn^{2+} -based PFDS NPs could be employed as excellent contrast agent for MR imaging. The PFDS NPs were labelled with ^{89}Zr for PET imaging. The ^{89}Zr -PFDS NPs could accumulate in the tumor and reduce liver uptake. Therefore, the PFDS NPs based nanoplatform could enhance the combination efficacy and reduce side effects on normal organs. Moreover, PFDS NPs could inhibit U87MG xenograft tumor growth owing to the high tumor accumulation of PFDS NPs. This polyphenols-based polymers nanoplatform is an excellent candidate for imaging guided cancer treatment. Our approach could be expanded to load various therapeutic agents in a wide range of clinical applications.

Supplementary Material

Refer to Web version on PubMed Central for supplementary material.

Acknowledgements

We gratefully acknowledge support from Intramural Research Program (IRP) of the National Institute of Biomedical Imaging and Bioengineering (NIBIB), National Institutes of Health (NIH), Faculty of Health Sciences, University of Macau, the Start-up Research Grant (SRG) of University of Macau (SRG2018-00130-FHS), and the Science and Technology Development Fund, Macau SAR (File no. FDCT 0109/2018/A3 to Y.D.).

References

1. Fan W, Yung B, Huang P and Chen X, *Chem. Rev*, 2017, 117, 13566–13638. [PubMed: 29048884]
2. Chen H, Zhang W, Zhu G, Xie J and Chen X, *Nat. Rev. Mater*, 2017, 2, 17024. [PubMed: 29075517]
3. Eetezadi S, Ekdawi SN and Allen C, *Adv. Drug Del. Rev*, 2015, 91, 7–22.
4. Seidi F, Jenjob R and Crespy D, *Chem. Rev*, 2018, 118, 3965–4036. [PubMed: 29533067]
5. Abdalla AME, Xiao L, Ullah MW, Yu M, Ouyang CX and Yang G, *Theranostics*, 2018, 8, 533–548. [PubMed: 29290825]
6. Dai Y, Cheng S, Wang Z, Zhang R, Yang Z, Wang J, Yung BC, Wang Z, Jacobson O, Xu C, Ni Q, Yu G, Zhou Z and Chen X, *ACS Nano*, 2018, 12, 455–463. [PubMed: 29293312]
7. Hwang GH, Min KH, Lee HJ, Nam HY, Choi GH, Kim BJ, Jeong SY and Lee SC, *Chem. Commun*, 2014, 50, 4351–4353.
8. Yang Z, Dai Y, Shan L, Shen Z, Wang Z, Yung BC, Jacobson O, Liu Y, Tang W, Wang S, Lin L, Niu G, Huang P and Chen X, *Nanoscale Horiz*, 2019, 4, 426–433.
9. Guo J, Ping Y, Ejima H, Alt K, Meissner M, Richardson JJ, Yan Y, Peter K, von Elverfeldt D, Hagemeyer CE and Caruso F, *Angew. Chem. Int. Ed*, 2014, 53, 5546–5551.
10. Ejima H, Richardson JJ and Caruso F, *Nano Today*, 2017, 12, 136–148.
11. Dai Y, Guo J, Wang T-Y, Ju Y, Mitchell AJ, Bonnard T, Cui J, Richardson JJ, Hagemeyer CE, Alt K and Caruso F, *Adv. Healthcare Mater*, 2017, 6, 1700467.
12. Shan L, Gao G, Wang W, Tang W, Wang Z, Yang Z, Fan W, Zhu G, Zhai K, Jacobson O, Dai Y and Chen X, *Biomaterials*, 2019, 210, 62–69. [PubMed: 31075724]
13. Dai Y, Yang Z, Cheng S, Wang Z, Zhang R, Zhu G, Wang Z, Yung BC, Tian R, Jacobson O, Xu C, Ni Q, Song J, Sun X, Niu G and Chen X, *Adv. Mater*, 2019, 30, 1704877.
14. Chen HJ, Niu G, Wu H and Chen XY, *Theranostics*, 2016, 6, 78–92. [PubMed: 26722375]
15. Siegel RL, Miller KD and Jemal A, *CA Cancer J. Clin*, 2017, 67, 7–30. [PubMed: 28055103]
16. Lammers T, Aime S, Hennink WE, Storm G and Kiessling F, *Acc. Chem. Res*, 2011, 44, 1029–1038. [PubMed: 21545096]
17. Luk BT, Fang RH and Zhang LF, *Theranostics*, 2012, 2, 1117–1126. [PubMed: 23382770]
18. Nitiss JL, *Nat. Rev. Cancer*, 2009, 9, 338. [PubMed: 19377506]
19. Wang Z, Dai Y, Wang Z, Jacobson O, Zhang F, Yung B, Zhang P, Gao H, Niu G, Liu G and Chen X, *Nanoscale*, 2018, 10, 1135–1141. [PubMed: 29271453]
20. Kaminsky YG and Kosenko EA, *Cent. Eur. J. Med*, 2010, 5, 269–279.
21. Ahn KS, Sethi G and Aggarwal BB, *Biochem. Pharmacol*, 2008, 75, 907–913. [PubMed: 18036510]
22. Safwat S, Hathout RM, Ishak RA and Mortada ND, *J. Liposome Res*, 2017, 27, 1–10. [PubMed: 26872624]
23. Fahmy UA and Aljaeid BM, *Expert Opin. Drug Deliv*, 2016, 13, 1653–1660. [PubMed: 27636370]
24. Ai S, Lin Y, Zheng J, Qiu C, Liu Y and Lin X, *Genet Mol. Res.: GMR*, 2016, 15, 15.
25. van der Spek E, Bloem AC, van de Donk N, Bogers LH, van der Griend R, Kramer MH, de Weerd O, Wittebol S and Lokhorst HM, *Haematol-Hematol. J*, 2006, 91, 542–545.
26. Werner M, Atil B, Sieczkowski E, Chiba P and Hohenegger M, *Naunyn-Schmiedeberg's Arch. Pharmacol*, 2013, 386, 605–617. [PubMed: 23564041]
27. Jochum FD, zur Borg L, Roth PJ and Theato P, *Macromolecules*, 2009, 42, 7854–7862.
28. Kim HW, McCloskey BD, Choi TH, Lee C, Kim M-J, Freeman BD and Park HB, *ACS Appl. Mater. Interfaces*, 2013, 5, 233–238. [PubMed: 23273315]
29. Kevadiya BD, Woldstad C, Ottemann BM, Dash P, Sajja BR, Lamberty B, Morsey B, Kocher T, Dutta R, Bade AN, Liu Y, Callen SE, Fox HS, Byrareddy SN, McMillan JM, Bronich TK, Edagwa BJ, Boska MD and Gendelman HE, *Theranostics*, 2018, 8, 256–276. [PubMed: 29290806]
30. Liu Y, Gong C, Lin L, Zhou Z, Liu Y, Yang Z, Shen Z, Yu G, Wang Z, Wang S, Ma Y, Fan W, He L, Niu G, Dai Y, Chen X, *Theranostics*, 2019, 9, 2791–2799. [PubMed: 31244923]
31. Yang Y, Liu J, Liang C, Feng L, Fu T, Dong Z, Chao Y, Li Y, Lu G, Chen M and Liu Z, *ACS Nano*, 2016, 10, 2774–2781. [PubMed: 26799993]

32. Miao Y, Xie Q, Zhang H, Cai J, Liu X, Jiao J, Hu S, Ghosal A, Yang Y, Fan H, *Theranostics*, 2019, 9, 1764–1776. [PubMed: 31037137]

Author Manuscript

Author Manuscript

Author Manuscript

Author Manuscript

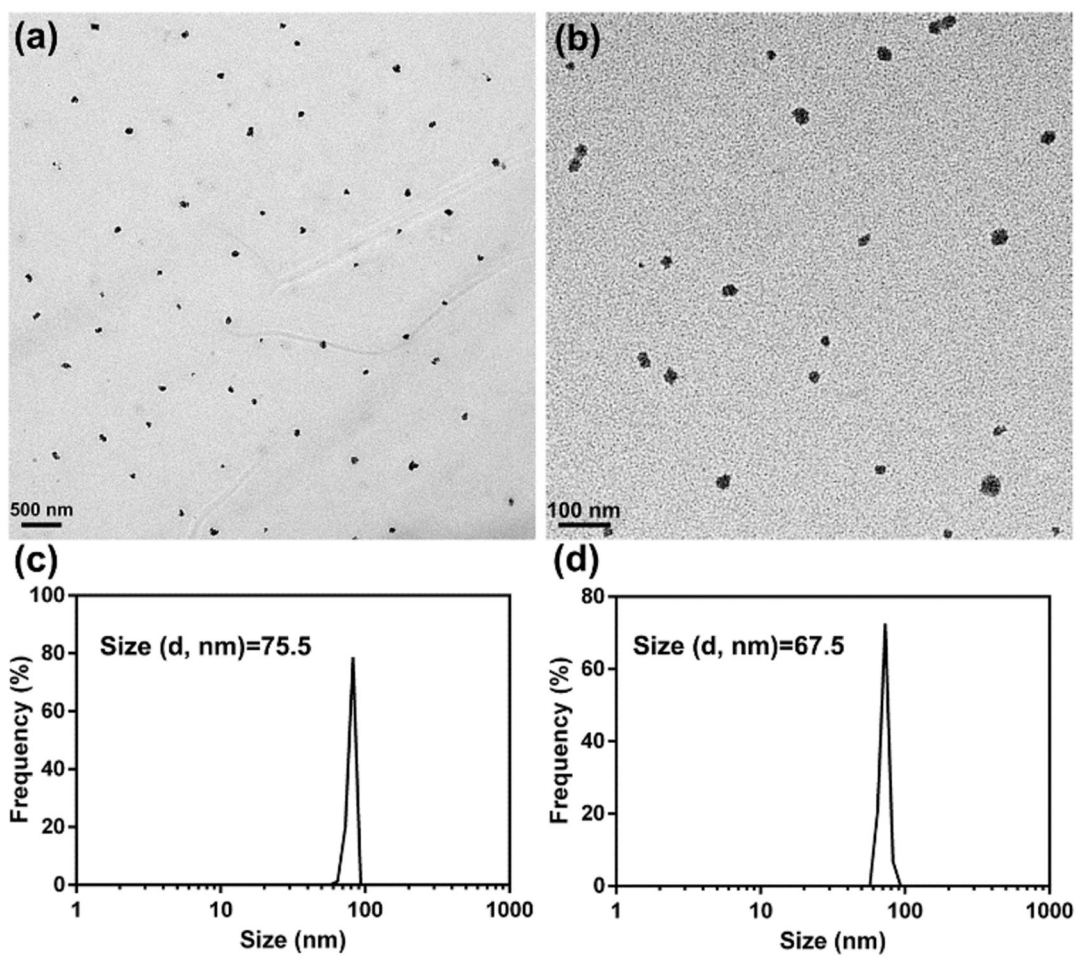


Fig. 1. TEM image of Fe³⁺ (a) and Mn²⁺ (b) based PFDS NPs, and the DLS of Fe³⁺ (c) and Mn²⁺ (d) based PFDS NPs in water.

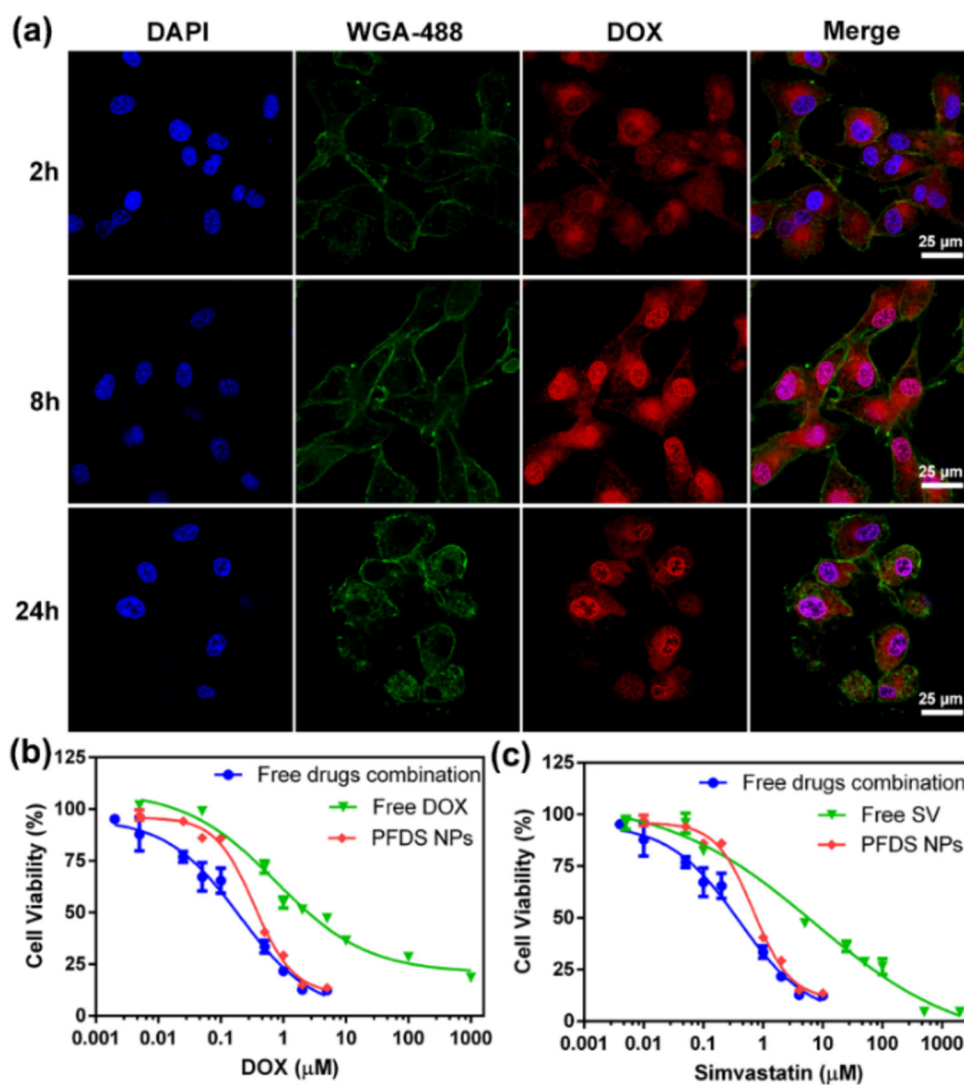


Fig. 2.

(a) Confocal microscopy images of DOX release from PFDS NPs under different incubation time. The nucleus and cell membrane were stained with DAPI, and Wheat Germ Agglutinin (WGA)-488, respectively, (b-c) the U87MG cell viability from different groups.

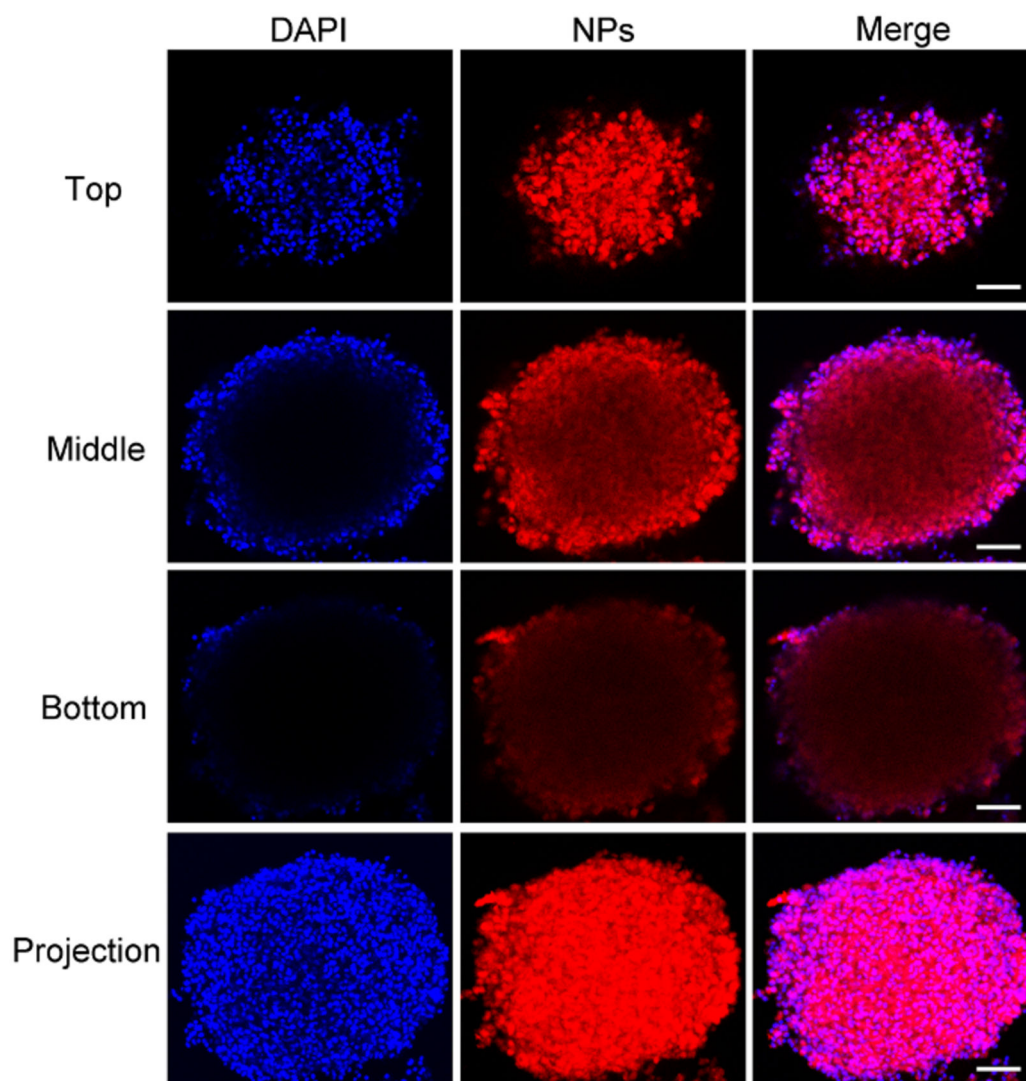


Fig. 3. Penetration of Ce6-labelled PFDS NPs in vitro. Representative confocal microscopy images from various layers (top, middle, and bottom), and the projection reconstructed from all the optical image sections. The scale bar: 100 μm .

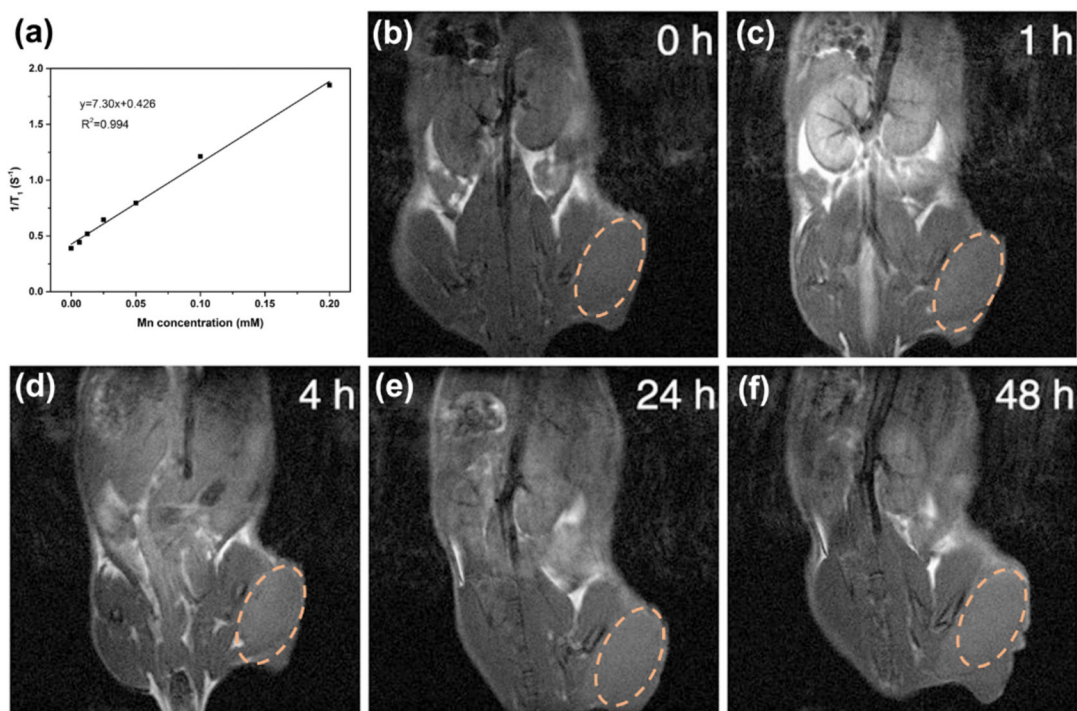


Fig. 4. (a) Relaxation rate r_1 versus different molar concentrations of Mn-based PFDS NPs. (b-f) T₁-weighted MR images of U87MG bearing nude mice pre- and post-intravenous injection of PFDS NPs. The dash circles indicate the tumor location.

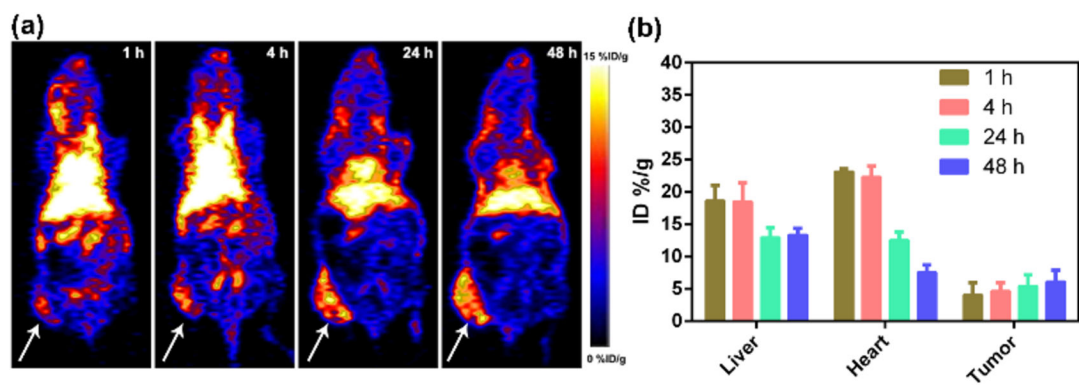


Fig. 5. (a) Whole-body PET images of the tumor-bearing mice and all the arrows show the tumor site. (b) The quantitative region of interest (ROI) analysis of PFDS NPs in liver, heart and tumor at various post-injection.

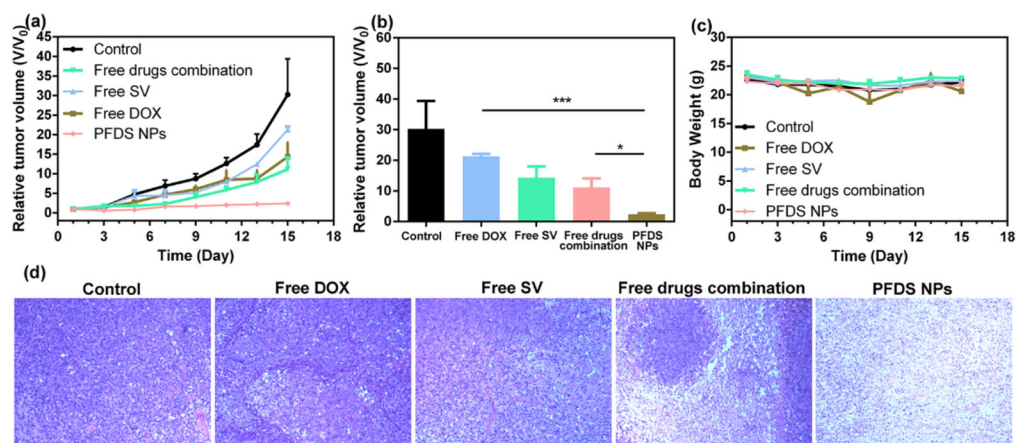
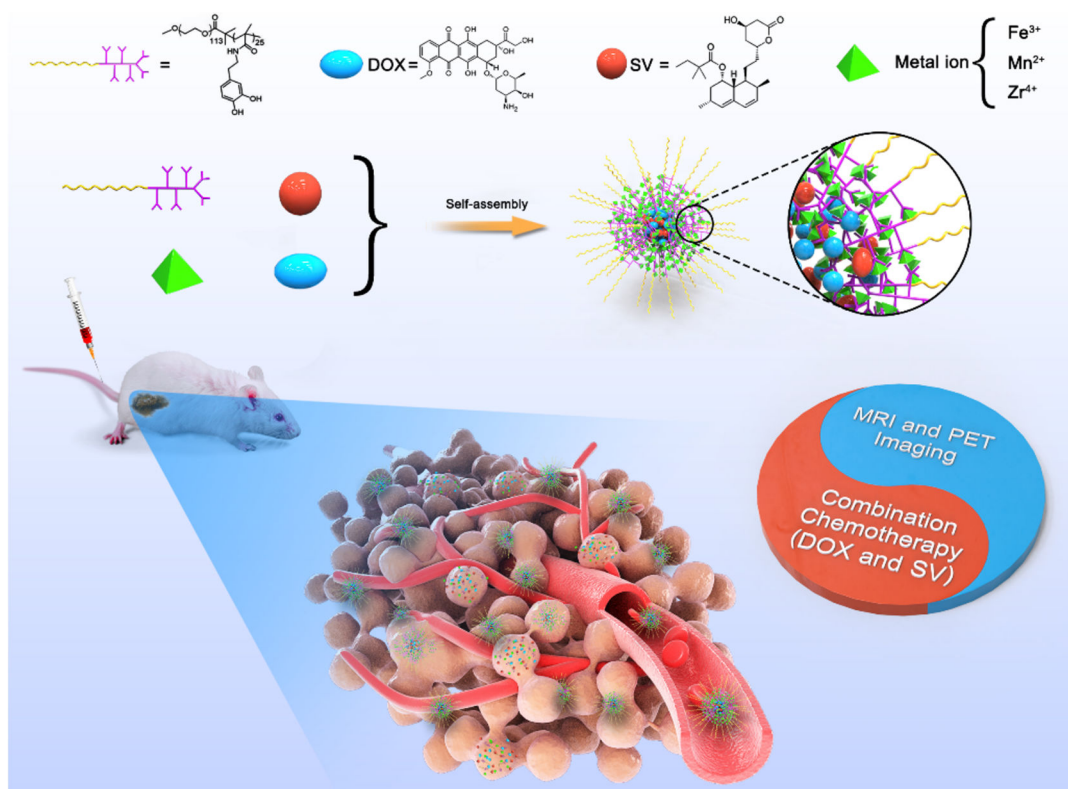


Fig. 6.

(a) U87MG tumor volume curves under from different groups, (b) the tumor size from different group on the 15th day (P values, $*P < 0.05$, $***P < 0.001$ by t -test.), (c) body weight of mice from different groups, and (d) H&E stained images of tumor sections after different treatments.

**Scheme 1.**

Preparation of PFDS NPs by self-assembly. The PFDS NPs can accumulate in the tumor and release two drugs for cancer theranostics.